arXiv:1511.01121v2 [physics.plasm-ph] 3 Feb 2016

Inverse Faraday Effect driven by Radiation Friction

T. V. Liseykina,[1,*] S. V. Popruzhenko,[2,†] and A. Macchi[3,4,‡]

[1] *Institute of Physics, University of Rostock, 18051 Rostock, Germany*
[2] *National Research Nuclear University, Moscow Engineering Physics Institute, Kashirskoe Shosse 31, 115409, Moscow, Russia*
[3] *CNR, National Institute of Optics (INO), Adriano Gozzini research unit, Pisa, Italy*
[4] *Enrico Fermi Department of Physics, University of Pisa, largo Bruno Pontecorvo 3, 56127 Pisa, Italy*

(Dated: February 4, 2016)

A collective, macroscopic signature to detect radiation friction in laser-plasma experiments is proposed. In the interaction of superintense circularly polarized laser pulses with high density targets, the effective dissipation due to radiative losses allows the absorption of electromagnetic angular momentum, which in turn leads to the generation of a quasistatic axial magnetic field. This peculiar "inverse Faraday effect" is investigated by analytical modeling and three-dimensional simulations, showing that multi-gigagauss magnetic fields may be generated at laser intensities $> 10^{23}$ W cm^{-2}.

The development of ultrashort pulse lasers with petawatt power has opened new perspectives for the study of high field physics and ultra-relativistic plasmas [1, 2]. In this context, the longstanding problem of radiation friction (RF) or radiation reaction has attracted new interest. RF arises from the back-action on the electron of the electromagnetic (EM) field generated by the electron itself and plays a dominant role in the dynamics of ultra-relativistic electrons in strong fields. A considerable amount of work has been devoted both to revisiting the RF theory [3] and to its implementation in laser-plasma simulations [4–8], as well as to the study of radiation-dominated plasmas in high energy astrophysics, see e.g. Refs.[9].

While RF is still an open matter both for classical and quantum electrodynamics [2], RF models have not been discriminated experimentally yet. This circumstance led to several proposals of devoted experiments providing clear signatures of RF, e.g. in nonlinear Thomson scattering [10], compton scattering [11], modification of Raman spectra [12], electron acceleration in vacuum [13], radiative trapping [14] or γ-ray emission from plasma targets [15]. Most of these studies are based on single particle effects, and RF signatures are found in modifications of observables such as emission patterns and spectra when RF is included in the modeling. Detecting such modifications may require substantial improvements in reducing typical uncertainities in laser-plasma experiments. Instead, in this Letter we propose to use a collective, macroscopic effect induced by RF, namely the generation of multi-gigagauss, quasi-steady, axial magnetic fields in the interaction of a circularly polarized (CP) laser pulse with a dense plasma. This is a peculiar form of the Inverse Faraday effect (IFE) [16] and may be more accessibile experimentally than single-particle effects. In fact, the IFE has been previously studied in different regimes of laser-plasma interactions [17–19, and references therein]. By using three-dimensional (3D) particle-in-cell (PIC) simulations, we find that at laser intensities foreseeable with next generation facilities producing multi-petawatt [20] or even exawatt pulses [21], the magnetic field created by the RF-driven IFE in dense plasma targets reaches multi-gigagauss values with a direction dependent on the laser polarization, which confirms its origin from the "photon spin". The magnetic field is slowly varying on times longer than the pulse duration and may be detected via optical polarimetry techniques [22], providing an unambiguous signature of the dominance of RF effects. The effect might also be exploited to create strongly magnetized laboratory plasmas in so far unexplored regimes (see e.g. [23]).

The IFE is due to absorption of EM angular momentum [24], which in general is *not* proportional to energy absorption. As an example of direct relevance to the present work, let us consider a mirror boosted by the radiation pressure of a CP (with positive helicity, for definiteness) laser pulse. From a quantum-mechanical point of view, the laser pulse of frequency ω propagating along $\hat{\mathbf{x}}$ corresponds to N incident photons with total energy $N\hbar\omega$ and angular momentum $N\hbar\hat{\mathbf{x}}$. If the mirror is perfect, N is conserved in any frame. If the mirror moves along $\hat{\mathbf{x}}$, the reflected photons are red-shifted leading to EM energy conversion into mechanical energy (up to 100% if the mirror velocity $\sim c$) but there is no spin flip for the reflected photons, hence no absorption of angular momentum. However, if the electrons in the mirror emit high-frequency photons, a greater number of incident low-frequency photons must be absorbed with their angular momentum. From a classical point of view, absorption of angular momentum requires some dissipation mechanism [19] which, in our example, implies a non-vanishing absorption in the rest frame of the mirror.

In the case here investigated, effective dissipation is provided by the RF force which makes the electron dynamics consistent with the radiative losses. In order to demonstrate IFE induced by RF, we consider a regime of ultra-high laser intensity $I_L > 10^{23}$ W cm^{-2} and thick plasma targets (i.e. with thickness much greater than the evanescence length of the laser field) where the radiative energy loss is a large fraction of the laser energy as shown

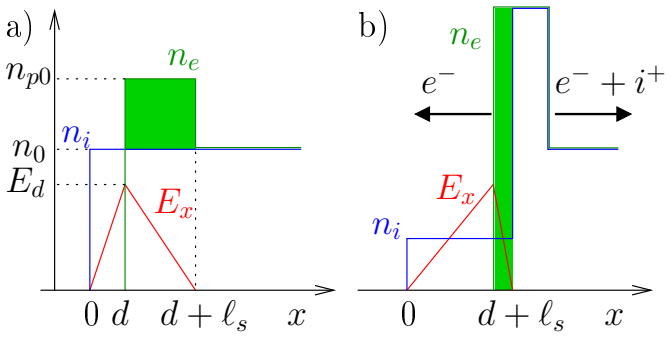

FIG. 1. (color online) Cartoon showing the electron dynamics during the "hole boring" stage. Frame a) shows the approximated profiles of the densities of ions (n_i) and electrons (n_e) and of the electrostatic field (E_x) at the early time ($t \simeq 0$) when ions have not moved yet and electrons from the depletion region ($0 < x < d$) pile up in the skin layer ($d < x < d+\ell_s$); the number of excess electrons N_x is proportional to the shaded area. Frame b) corresponds to the time $t \simeq \tau_i$ when the ions have reached the $x \simeq d+\ell_s$ position and formed a quasi-neutral bunch [30]; the excess electrons return towards the depletion region.

by simulations with RF included [25–28]. We use a simple model to account for such losses and provide a scaling law with the laser intensity. The power radiated by an electron moving with velocity v_x along the propagation axis of a CP pulse of amplitude $E_L = (m_e\omega c/e)a_0 \equiv B_0 a_0$ (with ω the laser frequency) is

$$P_{\rm rad} = \frac{2e^2\omega^2\gamma^2 a_0^2}{3c}\left(1-\frac{v_x}{c}\right)^2 . \qquad (1)$$

Since at the relevant frequencies $\omega_{\rm rad} \simeq a_0^2\omega$ the radiation is incoherent, the total radiated power by N comoving electrons will be $NP_{\rm rad}$. For thin targets accelerated by the CP laser pulse ("light sail" regime), all electrons move with the foil at $v_x \simeq c$, and there is no high-frequency oscillation driven by the $\mathbf{v}\times\mathbf{B}$ force. Thus the radiation is strongly suppressed by the factor $(1-v_x/c)^2 \ll 1$, as observed in simulations [6, 29]. In contrast, RF losses become very important for thick targets [25, 27, 28] ("hole boring" regime) because the acceleration of the plasma surface has a pulsed nature [26, 30, 31] with a dense bunch of electrons being periodically dragged towards the incident laser pulse, i.e. in a counterpropagating configuration ($v_x < 0$).

In order to estimate the number of radiating electrons per unit surface we consider the dynamic picture of hole boring [30, 32]. As illustrated in Fig.1, at the surface of the plasma the radiation pressure generates a positively charged layer of electron depletion (of thickness d) and a related pile-up of electrons in the skin layer (of thickness ℓ_s), i.e. the evanescent laser field region. Ions are accelerated in the skin layer leaving it at a time τ_i at which an ion bunch neutralized by accompanying electrons is formed. At this instant, the equilibrium between ponderomotive and electrostatic forces is lost and the excess electrons in the skin layer will quickly return back towards the charge depletion region. The number per unit surface of returning electrons is $N_x = (n_{p0}-n_0)\ell_s$ where n_{p0} is the electron density in the skin layer at the beginning of the acceleration stage. Using the model of Refs.[30, 32] N_x may be estimated from the balance of electrostatic and radiation pressures: $eE_d n_{p0}\ell_s/2 = 2I_L/c$ where $E_d = 4\pi e n_0 d$ is the peak field in the depletion region, and $n_{p0}\ell_s = n_0(d+\ell_s)$ because of charge conservation. Solving these equations in the limit $n_{p0} \gg n_0$ we obtain $N_x \simeq a_0/r_c\lambda$ where $\lambda = 2\pi c/\omega$ is the laser wavelength, $r_c = e^2/m_e c^2$ and we used $I_L = m_e c\omega^2 a_0^2/(4\pi r_c)$. Thus, the total radiated intensity is $I_{\rm rad} = P_{\rm rad}N_x$. In order to compare with the laser intensity I_L we take into account that the radiation is emitted as bursts corresponding to the periodic return of electrons towards the laser, i.e. for a fraction $f_\tau \simeq \tau_e/(\tau_e+\tau_i)$ of the interaction stage where τ_e is the time interval during which the electrons move backwards. Analysis of laser piston oscillations in Ref.[26] suggests that $\tau_e \simeq \tau_i$ so we take $f_\tau \simeq 1/2$ for our rough estimate. Assuming $(1-v_x/c)^2 \sim 1$ we obtain for the fraction of radiated energy to the laser pulse energy

$$\eta_{\rm rad} \simeq \frac{4\pi}{3}\frac{r_c}{\lambda}a_0\gamma^2 . \qquad (2)$$

If the energy of electrons is mainly due to the motion in the laser field, then $\gamma \simeq (1+a_0^2)^{1/2} \sim a_0$ for $a_0 \gg 1$ and $\eta_{\rm rad} \propto a_0^3$. For $\lambda = 0.8$ μm, $\eta_{\rm rad} \sim 1$ for $a_0 \sim 400$, corresponding to $I_L \sim 7\times 10^{23}$ W cm^{-2}. This order-of-magnitude estimate implies that for such intensities a significant part of the laser energy is lost as radiation, strongly affecting the interaction dynamics. A more precise estimate would require to account both for the energy depletion of the laser and for the trajectory modification of the electrons due to the RF force.

A 3D approach is essential to model the phenomena of angular momentum absorption and magnetic field generation, thus we rely on massively parallel PIC simulations in which RF is implemented following the approach described in Ref.[6] (see Ref.[8] for a benchmark with other approaches). The laser pulse is initialized in a way that at the waist plane $x = 0$ (coincident with the target boundary) the normalized amplitude of the vector potential $\mathbf{a} = e\mathbf{A}/m_e c^2$ would be

$$\mathbf{a}(x=0,r,t) = a_0\left(\hat{\mathbf{y}}\cos(\omega t) \pm \hat{\mathbf{z}}\sin(\omega t)\right) \times e^{-(r/r_0)^n-(ct/r_l)^4} , \qquad (3)$$

where $r = (y^2+z^2)^{1/2}$. Both radial profiles with $n = 2$ (Gaussian, G) and $n = 4$ (super-Gaussian, SG) have been used in the simulations. For all the results shown below, we take $r_l = 3\lambda$ and radius $r_0 = 3.8\lambda$. The plus and minus sign in the expression for $\mathbf{a}$ correspond to positive and negative helicity, respectively. The pulse energy is given

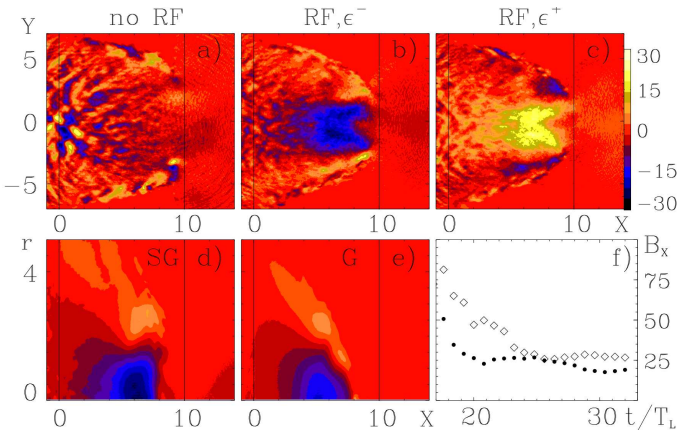

FIG. 2. (color online) a)-c): Axial magnetic field B_x (normalized to $B_0 = 1.34 \times 10^8$ G) in 3D simulation with a super-Gaussian pulse. Case a) is without RF, case b) c) are with RF included and for opposite helicities. The field is shown in the xy plane $t = 27\lambda/c$ after the beginning of the interaction (very similar patterns are observed in the xz plane, not shown). The laser pulse is incident along the x axis from the left side and the thin black lines denote the boundaries of the target. The coordinates are normalized to λ. d) and e): B_x averaged over the azimuthal direction comparison for Gaussian (G) and super-Gaussian (SG) pulse profiles. f): the temporal evolution of the maximum value of B_x on the x axis for both the G (filled dots) and SG (empty diamonds) pulses. The time $t = 0$ corresponds to the laser pulse peak reaching the waist, as in Eq.(3).

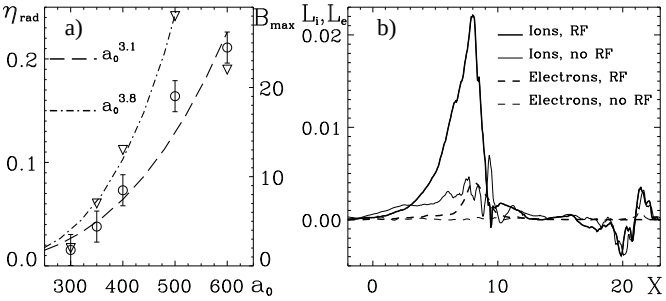

FIG. 3. a) Values of fractional radiative energy loss $\eta_{\rm rad}$ (circles) and maximum axial magnetic field $B_{\rm max}$ (triangles) as a function of laser amplitude a_0, from 3D simulations. The dashed and dash-dotted lines are fit to the data for $\eta_{\rm rad}$ and $B_{\rm max}$, respectively. The errorbars on $\eta_{\rm rad}$ correspond to the typical $\lesssim 1\%$ amount of energy which is not conserved in the simulation because of numerical errors. b) Axial angular momentum of electrons (dashed line) and ions (thick line) at $t = 27\lambda/c$. The density of angular momentum has been integrated over the radius and normalized to the total integrated angular momentum of the laser pulse. Results with and without RF included are shown.

by $U_L = \mathcal{A} r_0^2 r_l B_0^2 a_0^2$ where $\mathcal{A} = \Gamma(1/4) 2^{-17/2} \simeq 0.19$ and $\mathcal{A} = \pi^{1/2} \Gamma(1/4) 2^{-19/2} \simeq 0.24$ for the G and SG pulse cases, respectively. The target is a plasma of thickness 10λ and electron density $n_0 = 90 n_c$ (where $n_c = m_e \omega^2/(4\pi e^2)$ is the cut-off density) and charge-to-mass ratio for ions $Z/A = 1/2$. The range of laser amplitudes investigated in the simulation is $a_0 = 200 - 600$. Assuming $\lambda = 0.8\mu$m, the density $n_0 = 1.55 \times 10^{23}$ cm^{-3}, the pulse duration (full-width-half-maximum of the intensity profile) is 14.6 fs and the range for the peak laser intensity $I_L = m_e c^3 n_c a_0^2$ is $(1.9 - 16.7) \times 10^{23}$ W cm^{-2} corresponding to a pulse energy $U_L \simeq (0.38 - 3.4)$ kJ for the G pulse and $U_L \simeq (0.48 - 4.3)$ kJ for the SG pulse. The numerical box had a $30 \times 25 \times 25\lambda^3$ size, with 40 grid cells per λ and 64 particles per cell for each species. The simulations were performed on 480 cores of the JURECA supercomputer at Forschungszentrum Jülich.

Figures 2 a)-c) show the magnetic field B_x (normalized to $B_0 = 1.34 \times 10^8$ G for $\lambda = 0.8$ μm) along the propagation direction at time $t = 27\lambda/c$ for a simulation [a)] where RF is not included and for two simulations [b)-c)] including RF and having positive and negative helicity, respectively; the laser profile was super-Gaussian and $a_0 = 600$ in all the three simulations. Only with RF included an axial magnetic field of maximum amplitude $B_{\rm max} \simeq 22 B_0 = 2.9 \times 10^9$ G, extending over several microns and a polarity inverting with the pulse helicity is generated. The comparison of Fig.2 d) and e) shows that B_x has similar values and extension for a Gaussian pulse. The field is slowly varying over more than a ten laser cycles (∼30 fs) time, with no sign of rapid decay at the end of the simulation, as shown in Fig.2 f).

The fraction $\eta_{\rm rad}$ of the laser energy dissipated by RF reaches values up to $\eta_{\rm rad} \simeq 0.24$ for $a_0 = 600$ as shown in Fig.3 a) . A fit to the data gives $\eta_{\rm rad} \propto a_0^{3.1}$, close to the $\eta_{\rm rad} \sim a_0^3$ prediction of our model. Fig.3 a) also shows the peak magnetic field $B_{\rm max}$ scaling as $\sim a_0^{3.8}$ up to the highest value $B_{\rm max} \simeq 28 B_0 = 3.75$ GG for $a_0 = 500$. The decrease down to $B_{\rm max} \simeq 22 B_0$ for $a_0 = 600$ is related to the early interruption of the hole boring stage due to the breakthrough of the laser pulse through the target as observed in this case. Notice that we do not show simulations for $a_0 < 200$ since in such case the RF losses become too close to the percentage of energy which is lost due to numerical errors ($\lesssim 1\%$). However, the inferred scaling would predict $B_{\rm max} \sim 8$ MG for $a_0 = 100$, which may be still detectable making an experimental test closer. To sketch an analytical model for IFE, let us first observe that the density of angular momentum of the laser pulse $\mathcal{L}_z = \mathbf{r} \times (\mathbf{E} \times \mathbf{B})/4\pi c = -r \partial_r I_L(r)/(2c\omega)$, with $I_L(r)$ the radial profile of the intensity, vanishes on axis and has its maximum at the edge of the beam. We thus consider angular momentum absorption to occur in a thin cylindrical shell of radius $R \simeq r_0$, thickness $\delta \ll R$, and length h. The temporal growth of the axial field B_x induces an azimuthal electric field E_ϕ, which in turn allows the absorbed angular momentum to be transfered from electrons to ions. Assuming that the electron and ion shells rotate with angular velocities $\Omega_{e,i}$, respectively, we may

write for the angular momenta $L_e = \mathcal{I}_e\Omega_e$ and $L_i = \mathcal{I}_i\Omega_i$ where $\mathcal{I}_e = 2\pi R^3\delta h m_e n_e$ and $\mathcal{I}_i = (Am_p/Zm_e)\mathcal{I}_e$ are the momenta of inertia for electrons and ions, respectively. The global evolution of the angular momenta of electrons and ions may be described by the equations

$$\mathcal{I}_e\frac{d\Omega_e}{dt} = M_{\rm abs} - M_E\ , \qquad \mathcal{I}_i\frac{d\Omega_i}{dt} = M_E\ , \tag{4}$$

where $M_{\rm abs}$ is the torque due to angular momentum absorption (related to the absorbed power $P_{\rm abs}$ by $M_{\rm abs} = P_{\rm abs}/\omega$) and M_E is the torque due to E_ϕ:

$$M_E = \int eE_\phi(r) r n_e d^3r \simeq \frac{eE_\phi(R)}{m_e R}\mathcal{I}_e\ . \tag{5}$$

The rotation of the electrons induces a current density $j_{e\phi} \simeq -en_e\Omega_e R$. Neglecting the displacement current, in the limiting case $h \gg R$ the field $B_x \simeq 4\pi j_{e\phi}\delta/c$ and it is uniform as in a solenoid. In the opposite limit $h \sim \delta \ll R$, the current distribution may be approximated by a thin wire of cross-section $\sim h\delta$, and $E_\phi(R)$ can be obtained via the self-induction coefficient of a coil [33]. We thus obtain

$$M_E \simeq \mathcal{F}\frac{\omega_p^2 R\delta}{2c^2}\mathcal{I}_e\frac{d\Omega_e}{dt} \equiv \mathcal{I}'_e\frac{d\Omega_e}{dt}\ , \tag{6}$$

where $\omega_p^2 = 4\pi n_e e^2/m_e$. The geometrical factor $\mathcal{F} \simeq 1$ if $h \gg R$, and $\mathcal{F} \simeq (h/R)\ln(8R/\sqrt{h\delta})$ if $h \simeq \delta \ll R$. We thus obtain

$$\Omega_e(t) = \frac{1}{\mathcal{I}_e + \mathcal{I}'_e}\int_0^t M_{\rm abs}(t')dt'\ , \tag{7}$$

which shows that the electron rotation follows promptly the temporal profile of $M_{\rm abs}(t)$, and that effect of the inductive field on electrons is equivalent to effective inertia. Since in our conditions $\mathcal{I}'_e \sim (\omega_p^2/\omega^2)\mathcal{I}_e = (n_e/n_c)\mathcal{I}_e \gg \mathcal{I}_e$, the l.h.s. term in Eq.(4) can be neglected and $M_E \simeq M_{\rm abs}$ holds. Thus, from Eq.(4) we obtain

$$L_i \simeq \int_0^t M_{\rm abs}(t')dt' \simeq \frac{\mathcal{I}'_e}{\mathcal{I}_e}L_e \gg L_e\ , \tag{8}$$

i.e. the total angular momentum of ions is much larger that of electrons. This is in agreement with the simulation results [Fig.3 b)].

In turn, posing $M_E \simeq M_{\rm abs}$ in Eq.(5) and using $E_\phi(R) \simeq -(R/2c)\mathcal{G}\partial_t B_x(r=0,t)$ [where $\mathcal{G} = 1$ for $h \gg R$ and $\mathcal{G} \simeq (2/\pi)\ln(8R/\sqrt{h\delta})$ for $h \sim \delta \ll R$] we obtain for the final value of the magnetic field on axis $B_{xm} = B_x(r=0, t=\infty)$

$$\frac{\pi e}{c}n_e h R^3\delta\mathcal{G}B_{xm} \simeq \int_0^\infty M_{\rm abs}(t)dt = L_{\rm abs}\ . \tag{9}$$

The total angular momentum absorbed $L_{\rm abs} = U_{\rm abs}/\omega$ where the absorbed energy is $U_{\rm abs} \simeq \eta_{\rm rad}U_L$, assuming RF as the main source of dissipation. We thus estimate the final magnetic field as

$$\frac{B_{xm}}{B_0} \simeq \frac{\mathcal{A}}{\pi\mathcal{G}}\frac{\eta_{\rm rad}}{n_e h}\frac{B_0 c}{e\omega}\frac{r_l}{R\delta}a_0^2\ . \tag{10}$$

The product $n_e h$ is the surface density of the region where dissipation and angular momentum absorption occur. Thus, with reference to Fig.1 we may estimate $n_e h \simeq n_{p0}\ell_s \simeq (I_L/\pi e^2 c)^{1/2} = 2n_c a_0 c/\omega$ (for $n_{p0} \gg n_0$). Noticing that $B_0/en_c = 2\lambda$ we eventually obtain

$$\frac{B_{xm}}{B_0} \simeq \frac{\mathcal{A}}{\pi\mathcal{G}}\eta_{\rm rad}\frac{r_l\lambda}{R\delta}a_0\ . \tag{11}$$

If $\eta_{\rm rad} \propto a_0^3$ then $B_{xm} \propto a_0^4$, in good agreement with the observed scaling in Fig.3 a). If we pose $R \simeq r_0$, the laser initial beam radius, and $\delta \simeq \lambda$, the radial width of the angular momentum density, for $a_0 = 500$, $\eta_{\rm rad} = 0.16$ and $\mathcal{G} = 1$ Eq.(11) yields $B_{xm} \simeq 4.8B_0$. The discrepancy with the observed value of $\simeq 28B_0$ may be attributed to the nonlinear evolution and self-channeling of the laser pulse in the course of the hole boring process. For instance, Fig.2 shows that the magnetic field is generated in a region of radius $\sim 2\lambda$. Further analysis of the simulation data shows both a slight increase (by a factor ~ 1.2) of the laser amplitude on the axis and a localizaton of the densities of both EM and mechanical angular momenta in a narrow layer of $\sim 0.5\lambda$ width. Posing $R \simeq 2\lambda$, $\delta \simeq 0.5\lambda$ and an effective $a_0 \simeq 600$ in the above estimate yields $B_{xm} \simeq 23B_0$, which is in fair agreement with the simulation results considering the roughness of the model.

In conclusion, we showed in 3D simulations that in the interaction of superintense, circularly polarized laser pulses with thick, high density targets the strong radiation friction effects lead to angular momentum absorption and generation of multi-gigagauss magnetic fields via the Inverse Faraday effect. Simple models for the efficiency of radiative losses, the transfer of angular momentum to ions and the value of the magnetic field are in fair agreement with the simulation results for what concerns both the scaling with intensity and order-of-magnitude estimates. With the advent of multi-petawatt laser systems, the investigated effect may provide a laboratory example of radiation-dominated, strongly magnetized plasmas and a macroscopic signature of radiation friction, providing a test bed for related theories.

Suggestions from D. Bauer are gratefully acknowledged. The simulations were performed using the computing resources granted by the John von Neumann-Institut für Computing (Research Center Jülich) under the project HRO01. T.V.L. acknowledges DFG within the SFB 652. S.P. acknowledges support of the excellence center for applied mathematics and theoretical physics within MEPhI Academic Excellence Project (contract No. 02.a03.21.0005, 27.08.2013).

* On leave from Institute of Computational Technologies, SD-RAS, Novosibirsk, Russia; tatyana.liseykina@uni-rostock.de
† sergey.popruzhenko@gmail.com
‡ andrea.macchi@ino.it

[1] G. A. Mourou, T. Tajima, and S. V. Bulanov, "Optics in the relativistic regime," Rev. Mod. Phys. **78**, 309–371 (2006).

[2] A. Di Piazza, C. Müller, K. Z. Hatsagortsyan, and C. H. Keitel, "Extremely high-intensity laser interactions with fundamental quantum systems," Rev. Mod. Phys. **84**, 1177–1228 (2012).

[3] S. V. Bulanov, T. Zh. Esirkepov, M. Kando, J. K. Koga, and S. S. Bulanov, "Lorentz-Abraham-Dirac versus Landau-Lifshitz radiation friction force in the ultrarelativistic electron interaction with electromagnetic wave (exact solutions)," Phys. Rev. E **84**, 056605 (2011); Y. Kravets, A. Noble, and D. Jaroszynski, "Radiation reaction effects on the interaction of an electron with an intense laser pulse," *ibid.* **88**, 011201 (2013).

[4] A. Zhidkov, J. Koga, A. Sasaki, and M. Uesaka, "Radiation damping effects on the interaction of ultraintense laser pulses with an overdense plasma," Phys. Rev. Lett. **88**, 185002 (2002).

[5] I. V. Sokolov, N. M. Naumova, J. A. Nees, G. A. Mourou, and V. P. Yanovsky, "Dynamics of emitting electrons in strong laser fields," Phys. Plasmas **16**, 093115 (2009).

[6] M. Tamburini, F. Pegoraro, A. Di Piazza, C. H. Keitel, and A. Macchi, "Radiation reaction effects on radiation pressure acceleration," New J. Phys. **12**, 123005 (2010).

[7] M. Chen, A. Pukhov, T.-Pu Yu, and Z.-M. Sheng, "Radiation reaction effects on ion acceleration in laser foil interaction," Plasma Phys. Contr. Fusion **53**, 014004 (2011).

[8] M. Vranic, J. L. Martins, R. A. Fonseca, and L. O. Silva, "Classical Radiation Reaction in Particle-In-Cell Simulations," ArXiv e-prints (2015), arXiv:1502.02432 [physics.plasm-ph].

[9] C. H. Jaroschek and M. Hoshino, "Radiation-dominated relativistic current sheets," Phys. Rev. Lett. **103**, 075002 (2009); B. Cerutti, G. R. Werner, D. A. Uzdensky, and M. C. Begelman, "Simulations of particle acceleration beyond the classical synchrotron burnoff limit in magnetic reconnection: An explanation of the crab flares," The Astrophysical Journal **770**, 147 (2013); S. M. Mahajan, F. A. Asenjo, and R. D. Hazeltine, "Comparison of the electron-spin force and radiation reaction force," Mon. Not. Royal Astron. Soc. **446**, 4112–4115 (2015).

[10] J. Koga, T. Zh. Esirkepov, and S. V. Bulanov, "Nonlinear Thomson scattering in the strong radiation damping regime," Phys. Plasmas **12**, 093106 (2005); A. Di Piazza, K. Z. Hatsagortsyan, and C. H. Keitel, "Strong signatures of radiation reaction below the radiation-dominated regime," Phys. Rev. Lett. **102**, 254802 (2009); Y. Hadad, L. Labun, J. Rafelski, N. Elkina, C. Klier, and H. Ruhl, "Effects of radiation reaction in relativistic laser acceleration," Phys. Rev. D **82**, 096012 (2010); N. Neitz and A. Di Piazza, "Stochasticity effects in quantum radiation reaction," Phys. Rev. Lett. **111**, 054802 (2013); T. G. Blackburn, C. P. Ridgers, J. G. Kirk, and A. R. Bell, "Quantum radiation reaction in laser˘electron-beam collisions," *ibid.* **112**, 015001 (2014); M. Vranic, J. L. Martins, J. Vieira, R. A. Fonseca, and L. O. Silva, "All-optical radiation reaction at 10^{21} W/cm^2," *ibid.* **113**, 134801 (2014).

[11] J.-X. Li, K. Z. Hatsagortsyan, and C. H. Keitel, "Robust signatures of quantum radiation reaction in focused ultrashort laser pulses," Phys. Rev. Lett. **113**, 044801 (2014).

[12] N. Kumar, K. Z. Hatsagortsyan, and C. H. Keitel, "Radiation-reaction-force-induced nonlinear mixing of Raman sidebands of an ultraintense laser pulse in a plasma," Phys. Rev. Lett. **111**, 105001 (2013).

[13] M. Tamburini, C. H. Keitel, and A. Di Piazza, "Electron dynamics controlled via self-interaction," Phys. Rev. E **89**, 021201 (2014); D. G. Green and C. N. Harvey, "Transverse spreading of electrons in high-intensity laser fields," Phys. Rev. Lett. **112**, 164801 (2014); T. Heinzl, C. Harvey, A. Ilderton, M. Marklund, S. S. Bulanov, S. Rykovanov, C. B. Schroeder, E. Esarey, and W. P. Leemans, "Detecting radiation reaction at moderate laser intensities," Phys. Rev. E **91**, 023207 (2015).

[14] A. Gonoskov, A. Bashinov, I. Gonoskov, C. Harvey, A. Ilderton, A. Kim, M. Marklund, G. Mourou, and A. Sergeev, "Anomalous radiative trapping in laser fields of extreme intensity," Phys. Rev. Lett. **113**, 014801 (2014); L. L. Ji, A. Pukhov, I. Yu. Kostyukov, B. F. Shen, and K. Akli, "Radiation-reaction trapping of electrons in extreme laser fields," *ibid.* **112**, 145003 (2014); A. M. Fedotov, N. V. Elkina, E. G. Gelfer, N. B. Narozhny, and H. Ruhl, "Radiation friction versus ponderomotive effect," Phys. Rev. A **90**, 053847 (2014).

[15] T. Nakamura, J. K. Koga, T. Zh. Esirkepov, M. Kando, G. Korn, and S. V. Bulanov, "High-power γ-ray flash generation in ultraintense laser-plasma interactions," Phys. Rev. Lett. **108**, 195001 (2012); R. Capdessus, E. d'Humières, and V. T. Tikhonchuk, "Influence of ion mass on laser-energy absorption and synchrotron radiation at ultrahigh laser intensities," *ibid.* **110**, 215003 (2013).

[16] L. P. Pitaevskii, "Electric forces in a transparent dispersive medium," Sov. Phys. JETP **12**, 1008–1013 (1961); P. S. Pershan, "Nonlinear optical properties of solids: Energy considerations," Phys. Rev. **130**, 919–929 (1963); J. P. van der Ziel, P. S. Pershan, and L. D. Malmstrom, "Optically-induced magnetization resulting from the inverse Faraday effect," Phys. Rev. Lett. **15**, 190–193 (1965); J. Deschamps, M. Fitaire, and M. Lagoutte, "Inverse Faraday effect in a plasma," *ibid.* **25**, 1330–1332 (1970).

[17] A. D. Steiger and C. H. Woods, "Intensity-dependent propagation characteristics of circularly polarized high-power laser radiation in a dense electron plasma," Phys. Rev. A **5**, 1467 (1972); A. S. Abdullaev and A. A. Frolov, "The inverse Faraday effect in a relativistic electron plasma," Sov. Phys. JETP **54**, 493 (1981); V. Yu. Bychenkov, V. I. Demin, and V. T. Tikhonchuk, "Electromagnetic field generation by an ultrashort laser pulse in a rarefied plasma," JETP **78**, 62 (1994); Z. M. Sheng and J. Meyer-ter-Vehn, "Inverse Faraday effect and propagation of circularly polarized intense laser beams in plasmas," Phys. Rev. E **54**, 1833–1842 (1996); V. I. Berezhiani, S. M. Mahajan, and N. L. Shatashvili, "Theory of magnetic field generation by relativistically strong laser radiation," *ibid.* **55**, 995 (1997).

[18] M. G. Haines, "Generation of an axial magnetic field from

photon spin," Phys. Rev. Lett. **87**, 135005 (2001).

[19] G. Shvets, N. J. Fisch, and J.-M. Rax, "Magnetic field generation through angular momentum exchange between circularly polarized radiation and charged particles," Phys. Rev. E **65**, 046403 (2002).

[20] C. Danson, D. Hillier, N. Hopps, and D. Neely, "Petawatt class lasers worldwide," High Power Laser Science and Engineering **3**, e3 (2015).

[21] G.A. Mourou, N.J. Fisch, V.M. Malkin, Z. Toroker, E.A. Khazanov, A.M. Sergeev, T. Tajima, and B. Le Garrec, "Exawatt-zettawatt pulse generation and applications," Optics Comm. **285**, 720 – 724 (2012); G. Mourou, B. Brocklesby, T. Tajima, and J. Limpert, "The future is fibre accelerators," Nat. Photonics **7**, 258–261 (2013).

[22] Y. Horovitz, S. Eliezer, A. Ludmirsky, Z. Henis, E. Moshe, R. Shpitalnik, and B. Arad, "Measurements of inverse Faraday effect and absorption of circularly polarized laser light in plasmas," Phys. Rev. Lett. **78**, 1707–1710 (1997); M. Borghesi, A. J. Mackinnon, R. Gaillard, O. Willi, A. Pukhov, and J. Meyer-ter Vehn, "Large quasistatic magnetic fields generated by a relativistically intense laser pulse propagating in a preionized plasma," *ibid.* **80**, 5137 (1998); Z. Najmudin, M. Tatarakis, A. Pukhov, E. L. Clark, R. J. Clarke, A. E. Dangor, J. Faure, V. Malka, D. Neely, M. I. K. Santala, and K. Krushelnick, "Measurements of the inverse Faraday effect from relativistic laser interactions with an underdense plasma," *ibid.* **87**, 215004 (2001); M. Tatarakis, I. Watts, F. N. Beg, E. L. Clark, A. E. Dangor, A. Gopal, M. G. Haines, P. A. Norreys, U. Wagner, M.-S. Wei, M. Zepf, and K. Krushelnick, "Laser technology: Measuring huge magnetic fields," Nature **415**, 280 (2002); U. Wagner, M. Tatarakis, A. Gopal, F. N. Beg, E. L. Clark, A. E. Dangor, R. G. Evans, M. G. Haines, S. P. D. Mangles, P. A. Norreys, M.-S. Wei, M. Zepf, and K. Krushelnick, "Laboratory measurements of 0.7 GG magnetic fields generated during high-intensity laser interactions with dense plasmas," Phys. Rev. E **70**, 026401 (2004).

[23] S. Eliezer, P. Norreys, J. T. Mendonça, and K. Lancaster, "Effects of Landau quantization on the equations of state in intense laser plasma interactions with strong magnetic fields," Phys. Plasmas **12**, 052115 (2005).

[24] Here we consider only the absorption of intrinsic angular momentum or photon "spin". For studies on orbital angular momentum absorption and IFE in laser-plasma interaction see, e.g., Refs.[34].

[25] N. Naumova, T. Schlegel, V. T. Tikhonchuk, C. Labaune, I. V. Sokolov, and G. Mourou, "Hole boring in a DT pellet and fast-ion ignition with ultraintense laser pulses," Phys. Rev. Lett. **102**, 025002 (2009).

[26] T. Schlegel, N. Naumova, V. T. Tikhonchuk, C. Labaune, I. V. Sokolov, and G. Mourou, "Relativistic laser piston model: Ponderomotive ion acceleration in dense plasmas using ultraintense laser pulses," Phys. Plasmas **16**, 083103 (2009).

[27] R. Capdessus, M. Lobet, E. d'Humières, and V. T. Tikhonchuk, "γ-ray generation enhancement by the charge separation field in laser-target interaction in the radiation dominated regime," Phys. Plasmas **21**, 123120 (2014); R. Capdessus and P. McKenna, "Influence of radiation reaction force on ultraintense laser-driven ion acceleration," Phys. Rev. E **91**, 053105 (2015).

[28] E. N. Nerush and I. Y. Kostyukov, "Laser-driven hole boring and gamma-ray emission in high-density plasmas," Plasma Phys. Contr. Fusion **57**, 035007 (2015).

[29] M. Tamburini, T. V. Liseykina, F. Pegoraro, and A. Macchi, "Radiation-pressure-dominant acceleration: Polarization and radiation reaction effects and energy increase in three-dimensional simulations," Phys. Rev. E **85**, 016407 (2012).

[30] A. Macchi, F. Cattani, T. V. Liseykina, and F. Cornolti, "Laser acceleration of ion bunches at the front surface of overdense plasmas," Phys. Rev. Lett. **94**, 165003 (2005).

[31] T. Schlegel and V. T. Tikhonchuk, "Classical radiation effects on relativistic electrons in ultraintense laser fields with circular polarization," New J. Phys. **14**, 073034 (2012).

[32] A. Macchi, "A superintense laser-plasma interaction theory primer," (Springer, 2013) Chap. 5.7.2.

[33] J. D. Jackson, "Classical electrodynamics," (Wiley, New York, NY, 1999) Chap. 5, 3rd ed., prob. 5.32.

[34] S. Ali, J. R. Davies, and J. T. Mendonca, "Inverse Faraday effect with linearly polarized laser pulses," Phys. Rev. Lett. **105**, 035001 (2010); W. Wang, B. Shen, X. Zhang, L. Zhang, Y. Shi, and Z. Xu, "Hollow screw-like drill in plasma using an intense Laguerre-Gaussian laser," Scient. Rep. **5**, 8274 (2015).